

Diffusion symmetries of non-rigid shapes

Dan Raviv

Technion – Israel Institute of Technology

darav@cs.technion.ac.il

Michael M. Bronstein

Technion – Israel Institute of Technology

mbron@cs.technion.ac.il

Alexander M. Bronstein

Technion – Israel Institute of Technology

bron@cs.technion.ac.il

Ron Kimmel

Technion – Israel Institute of Technology

ron@cs.technion.ac.il

Guillermo Sapiro

University of Minnesota

guille@umn.edu

Abstract

Detection and modeling of self-similarity and symmetry is important in shape recognition, matching, synthesis, and reconstruction. While the detection of rigid shape symmetries is well-established, the study of symmetries in non-rigid shapes is a much less researched problem. A particularly challenging setting is the detection of symmetries in non-rigid shapes affected by topological noise and asymmetric connectivity. In this paper, we treat shapes as metric spaces, with the metric induced by heat diffusion properties, and define non-rigid symmetries as self-isometries with respect to the diffusion metric. Experimental results show the advantage of the diffusion metric over the previously proposed geodesic metric for exploring intrinsic symmetries of bendable shapes with possible topological irregularities.

1. Introduction

Symmetry or geometric self-similarity plays a fundamental role in Nature and is tightly tied to shape analysis and understanding. The exact definition of symmetry heavily depends on what we understand by the geometry of the shape. Broadly speaking, intrinsic geometry describes the properties of the shape which are invariant to inelastic deformations, while extrinsic geometry is associated with rigid transformations. In the pattern recognition and computer vision literature, there exists a significant number of papers dedicated to finding symmetries in images [24], and two-dimensional [1, 2] and three-dimensional shapes [19, 27, 29, 30]. Traditionally, symmetries are described by extrinsic geometry using rotations and reflections. While being adequate for rigid shapes, such a description is in-

appropriate for non-rigid ones. Extrinsic symmetry can be broken as a result of shape deformations such as bends, while its intrinsic symmetry is preserved [32, 33].

While finding shape representations that are invariant to bending has been intensively studied in recent years [5, 11, 13, 15, 16, 23, 25, 26, 35, 37], very little has been done in the research of regularity and self-similarity of non-rigid shapes. Raviv *et al.* [32] first defined and proposed a computational framework of exploring exact and approximate intrinsic self-similarities via the consideration of geodesic distances. They used the numerical scheme presented in [5, 6] for computation of minimum-distortion correspondence between metric spaces. In [29] Ovsjanikov *et al.* showed how eigenfunctions of the Laplace-Beltrami operator can be used for identifying reflective symmetries. They transformed intrinsic symmetries to (approximate) Euclidean ones in a feature space created by the Laplace-Beltrami eigenfunctions. The reader is also referred to recent papers on such spectral signatures [3, 20, 34, 35, 37]. Xu *et al.* [39] showed how a voting scheme can be used to find partial reflective symmetry in 3D shapes and how to use such symmetries for mesh segmentation and part repair. Topology and connectivity changes resulting e.g. from noise and acquisition artifacts can have a dramatic influence on intrinsic geometry defined by the geodesic distances. Since the geodesic is the shortest path, even a small change in the topology can cause a significant change in the geodesic metric by affecting the length of many geodesics, thus the approach proposed in [32] is sensitive to topology changes. Ovsjanikov *et al.* [29] explain why topology noise appears in high frequencies, hence its influence can be reduced in their method. Yet, they can not guarantee robustness to major topology changes.

In [8] it was shown that diffusion geometry, arising from the study of heat propagation on the surface, can gracefully handle topological and connectivity problems. In this paper we introduce *diffusion symmetries* of non-rigid shapes which are robust to topology changes. We apply [8] topology aware embeddings for the topology robust exploration of self-similarities.

The rest of this paper is organized as follows: In Section 2, we present the mathematical background of diffusion geometry. In Section 3, we define exact and approximate diffusion symmetries. followed by Section 4 where we elaborate on Gromov-Hausdorff distance. Section 5 is dedicated for the numerical framework, followed by Section 6 where we present experimental results. Section 7 concludes the paper.

2. Diffusion geometry

Well-known in other fields for decades, diffusion geometry has been popularized in data analysis by Lafon and Coifman [10, 21]. Informally, the diffusion distances have an effect of averaging over all possible paths connecting two points, while the geodesic distance is the length of just the minimal one. As a consequence, the former is more robust than the geodesic distance in cases where topological changes are present [28, 38].

Formally, the diffusion distance, is related to the *heat equation*,

$$\left(\Delta_X + \frac{\partial}{\partial t}\right) u = 0, \quad (1)$$

governing the distribution of heat u on the surface. Here, Δ_X denotes the *Laplace-Beltrami operator*, a generalization of the Laplacian to non-Euclidean domains. (Note that we define Δ_X as a positive-semidefinite operator, hence its positive sign in (1)). The fundamental solution $h_t(x, z)$ of the heat equation (1), also called the *heat kernel*, is the solution with a point heat source at $x \in X$ used as the initial condition at $t = 0$. The heat kernel $h_t(x, z)$ describes the heat distribution at time t at point $z \in X$.

For compact manifolds, the Laplace-Beltrami operator has discrete eigendecomposition of the form

$$\Delta_X \phi_i = \lambda_i \phi_i, \quad (2)$$

where $\lambda_0, \lambda_1, \dots$ are eigenvalues and ϕ_0, ϕ_1, \dots are the corresponding eigenfunctions. Using this basis, the heat kernel can be presented as [18]

$$h_t(x, z) = \sum_{i=0}^{\infty} e^{-\lambda_i t} \phi_i(x) \phi_i(z) \quad (3)$$

Note that for a single connected component $\lambda_0 = 0$, $\lambda_i \geq 0$ and $\phi_0 = \text{const}$.

The diffusion distance is the family of metrics

$$\begin{aligned} d_{X,t}^2(x, y) &= \|h_t(x, \cdot) - h_t(y, \cdot)\|_{L_2(X)}^2 \quad (4) \\ &= \int_X |h_t(x, z) - h_t(y, z)|^2 dz \\ &= \sum_{i=1}^{\infty} e^{-2\lambda_i t} (\phi_i(x) - \phi_i(y))^2, \end{aligned}$$

parametrized by scale t . Since the diffusion distance is derived from the Laplace-Beltrami operator which is an intrinsic property of the shape, it is an intrinsic metric and is therefore bending-invariant.

3. Symmetry

The metric model of shapes allows to formalize the notions of invariance, self-similarity, and symmetry. From the metric viewpoint, a shape is invariant under a transformation if the metric structure is unaffected by the transformation. More formally, two shapes (X, d) and (Y, \tilde{d}) , where d, \tilde{d} are the respective metric, are *isometric* if there exists a bijective map $\varphi : X \rightarrow Y$ (called *isometry*) such that $\tilde{d} \circ (\varphi \times \varphi) = d$. In particular, the shape (X, d) is *self-similar* or *self-isometric* if there exists a *permutation* (bijective map f from X to itself) which is an isometry with respect to d , i.e., $d \circ (f \times f) = d$.

It can be easily shown that symmetries form a subgroup of the group of permutations $(\Pi(X), \circ)$, where $\Pi(X) = \{g : X \xrightarrow{1:1} X\}$ and \circ is the function composition operator. We denote the group of symmetries of X by

$$\text{Sym}(X, d) = \{f \in \Pi(X) : d \circ (f \times f) = d\}. \quad (5)$$

3.1. Approximate symmetries

Because the true symmetry is a idealized rather than naturally occurring phenomenon, a relaxation of the notion of symmetry is required [40]. In the Euclidean case, *approximate symmetry* can be defined as a non-trivial Euclidean transformation i satisfying $i(X) \approx X$. In the more general setting, the relaxation of the notion of symmetry is possible by allowing $d \circ (f \times f) \approx d$ in the definition of self-isometry. More formally, we say that the shape (X, d) is ϵ -*self-isometric* if there exists a permutation $f \in \Pi(X)$ with *distortion*

$$\begin{aligned} \text{dis}(f, d) &= \|d \circ (f \times f) - d\|_{\infty} \quad (6) \\ &= \max_{x, x' \in X} |d(x, x') - d(f(x), f(x'))| \leq \epsilon. \end{aligned}$$

We denote the family of all ϵ -self-isometries of (X, d) by

$$\text{Iso}_{\epsilon}(X, d) = \{f \in \Pi(X) : \text{dis}(g, f) \leq \epsilon\}. \quad (7)$$

In particular, for $\epsilon = 0$ we get the symmetry group $\text{Iso}_0(X, d) = \text{Iso}(X, d)$. Note that unlike $\text{Iso}(X, d)$,

$\text{Iso}_\epsilon(X, d)$ is not a group for $\epsilon > 0$, since it does not satisfy the closure property: a composition of two ϵ -self-isometries is in general a 2ϵ -self-isometry.

3.2. Local asymmetry

In many cases, the shape asymmetry is as important as symmetry, as it indicates some abnormality of a shape. Given an ϵ -symmetric shape and one of its approximate symmetries $f \in \text{Iso}_\epsilon(X, d)$, we can compute the contribution of each point to the shape asymmetry as the *local shape asymmetry*,

$$\text{asym}_{(X,d)}(f, x) = \max_{x' \in X} |d_X(x, x') - d_X(f(x), f(x'))|, \quad (8)$$

quantifying the distortion of f at a point x . Points with large local asymmetry are responsible for symmetry breaking. *Global shape asymmetry* can be calculated as the supremum of all local ones, which is the same as the distortion $\text{dis}(f, d)$.

3.3. Symmetry space

Though we cannot use a group structure to represent approximate symmetries, we can still explore the space of permutation $\Pi(X)$, where each function g has its distortion $\text{dis}(g, d)$.

The space of functions $\Pi(X)$ can also be endowed with a standard metric that measures the distance between two permutations f and g on X , defined as

$$d_{\Pi(X)}(f, g) = \max_{x \in X} d(f(x), g(x)) = d(f(X), g(X)), \quad (9)$$

which, in turn, depends on the choice of the metric d . We refer to the set

$$B_{\Pi(X)}(g, r) = \{f \in \Pi(X) : d_{\Pi(X)}(g, f) \leq r\} \quad (10)$$

as the *closed metric ball* (intrinsic or extrinsic, according to the choice of the metric in the definition of $d_{\Pi(X)}$) of radius r centered at g . (We will omit r referring to a ball of some unspecified radius).

Since true symmetries do not have any distortion (i.e. $\text{dis}(g, d) = 0$), they are the global minimizers of the distortion function $\text{dis}(g, d)$. Moreover, they are also *local minimizers* of the distortion, in the sense that for every approximate symmetry g , there exists a sufficiently small neighborhood $B_{\Pi(X)}(g)$, such that any $f \in B_{\Pi(X)}(g)$, $\text{dis}(f) \geq \text{dis}(g)$. While trivial for true symmetries, this description motivates our selection of local minima for approximate symmetries, even when the distortion does not vanish.

We therefore define approximate symmetries as

$$\text{Sym}_\epsilon(X, d) = \{g \in \text{Iso}_\epsilon(X, d) : \text{dis}(g, d) \leq \text{dis}(f, d) \forall f \in B_{\Pi(X)}(g)\}. \quad (11)$$

Numerically, we observed that for a small ϵ , the number of local minima is similar to the number of true symmetries of a symmetric shape.

4. Gromov-Hausdorff distance

An early attempt to compare shapes as metric spaces was done by Elad and Kimmel [11] who proposed to embed pairwise geodesic distances into a third fixed metric space (Z, d_Z) . Usually, a low dimension Euclidean space is a good candidate from the computational point of view. Such a minimum distortion embedding was referred to as *canonical form*, and can be explicitly calculated by minimizing

$$\min_{\varphi: X \rightarrow Z} \max_{x, x' \in X} |d_X(x, x') - d_Z(\varphi(x), \varphi(x'))|. \quad (12)$$

Assuming the embedding distortion is low enough, the comparison of (X, d_X) and (Y, d_Y) can be reduced to rigid matching of canonical forms, e.g. using the *Hausdorff distance*,

$$d_H^Z(\varphi(X), \psi(Y)) = \max\left\{ \max_{y \in \psi(Y)} \min_{x \in \varphi(X)} d_Z(x, y), \max_{x \in \varphi(X)} \min_{y \in \psi(Y)} d_Z(x, y) \right\}. \quad (13)$$

A general theoretical framework for metric spaces comparison was proposed by Gromov [9, 15], and introduced to shape analysis by Mémoli and Sapiro [26]. Since it is generally impossible to select a common metric space (Z, d_Z) accommodating all shapes, Gromov suggested to optimize also for Z , resulting in the following distance, referred to as the *Gromov-Hausdorff distance*,

$$d_{GH}(X, Y) = \inf_{\substack{\varphi: X \rightarrow Z \\ \psi: Y \rightarrow Z \\ Z}} d_H^Z(\varphi(X), \psi(Y)), \quad (14)$$

where ψ and φ are isometric mappings. The Gromov-Hausdorff distance can be alternatively expressed in terms of correspondences between the two metric spaces [9] as

$$d_{GH}(X, Y) = \frac{1}{2} \inf_C \text{dis}(C), \quad (15)$$

where $C \subset X \times Y$ is a correspondence between the spaces, and $\text{dis}(C)$ is its distortion

$$\text{dis}(C) = \sup_{(x,y), (x',y') \in C} |d_X(x, x') - d_Y(y, y')|. \quad (16)$$

Note that for C to be a valid correspondence, for each $x \in X$ there must exist at least one $y \in Y$ such that $(x, y) \in C$, and vice versa for each $y \in Y$ there must exist at least one $x \in X$ such that $(x, y) \in C$.

In [5] it was shown how (15) can be efficiently approximated using a convex optimization framework. In this paper, we adopt this scheme for the computation of self-isometries.

5. Numerical framework

For practical computation of symmetries, the surface X has to be discretized and sampled at N points, constituting an r -covering (i.e., $X = \bigcup_{n=1}^N B_X(x_n, r)$, where B_X denotes a closed ball on X induced by the metric d_X). We denote this sampling by $X_r = \{x_1, \dots, x_N\} \subseteq X$. A good sampling strategy can be achieved using the (2 optimal) *farthest point sampling* algorithm [17], which guarantees that X_r is also r -separated, i.e. $d_{X,t}(x_i, x_j) \geq r$ for any $i \neq j$. X is approximated by a triangular mesh \hat{X} built upon the vertices X_r .

5.1. Approximation of distances

The diffusion metric is computed according to (4). For this purpose, we first compute the discrete approximation of the Laplace-Beltrami operator on the mesh, which has the following generic form

$$(\Delta_{\hat{X}} f)_i = \frac{1}{a_i} \sum_j w_{ij} (f_i - f_j), \quad (17)$$

where $f : \hat{X} \rightarrow \mathbb{R}$ is a scalar function defined on the mesh \hat{X} and represented as a vector of function values at the vertices of the mesh, w_{ij} are weights, and a_i are normalization coefficients. In matrix notation, Equation (17) can be written as

$$\Delta_{\hat{X}} f = A^{-1} L f, \quad (18)$$

where $A = \text{diag}(a_i)$ and $L = \text{diag}(\sum_{l \neq i} w_{il}) - (w_{ij})$.

There exists several discretizations of the Laplace-Beltrami operator [4, 12, 34, 41], for which A and L are defined. Here we adopt the *cotangent weight* scheme [31], in which a_i is set to be half of the area of the circumcentric dual of vertex i , and $w_{ij} = \cot \alpha_{ij} + \cot \beta_{ij}$, where α_{ij} and β_{ij} are the angles opposite to the edge between the i 'th and j 'th vertices, if one exists and zero otherwise.

By solving the *generalized eigendecomposition* problem [22]

$$L \phi = \lambda A \phi, \quad (19)$$

the k smallest eigenvalues $\lambda_0, \dots, \lambda_k$ and corresponding eigenfunctions $\phi_0, \dots, \phi_k : \hat{X} \rightarrow \mathbb{R}$ of the discretized Laplace-Beltrami operator are computed.

5.2. Coarse matching

Discrete permutations on X_r can be represented as N -tuples of the form $\pi = (\pi_1, \dots, \pi_N) \in \{1, \dots, N\}^N$. Finding all permutations with a distortion lower than ϵ requires computation of the distortion of $\mathcal{O}(N!)$ possible mappings. However, the search space can be greatly reduced by ruling out mappings that can not have low distortion. We observe that for a good candidate of an approximate symmetry, the

intrinsic properties of the surface, such as local intrinsic geometry around x_i should be similar to that around x_{π_i} . In order to quantify this behavior, for each $x_i \in X_r$ we compute the histogram $h_i = \text{hist}(\{\hat{d}_{ij} : \hat{d}_{ij} \leq \rho\})$ of the approximate distances ($\hat{d}_{ij} = d_X(x_i, x_j)$) in a ρ -ball centered at x_i [14, 23, 32].

In order to reduce the number of possible permutations we chose a small number of points to represent the symmetry using *farthest point sampling* strategy on diffusion distances. Experiments showed that resampling the surface starting from the second sampled point produces a better sampling because the location of the first point is arbitrary and its support may occlude a better one. Each point has many possible matches and clustering of the candidates is performed. Two points are in the same cluster if and only if there exists a chain of points on the surface with similar distance histograms. Earth mover's distance [36] can be used as the distance between histograms.

For a given point x we compute its histogram h_x and find all points y with a similar histogram, denoted by

$$H_\delta(x) = \{y : d(h_x, h_y) \leq \delta\}, \quad (20)$$

where d is the distance between the histograms, and δ is calculated a priori according to the histogram distance between neighboring points. We perform ϵ separation of the set $H_\delta(x)$ to subsets $H_\delta^i(x)$ according to

$$\begin{aligned} y, z \in H_\delta^i(x) & \quad \text{iff } y, z \in H_\delta(x) \text{ and } \exists \{y_k\}_1^m \in H_\delta(x) \\ & \quad \text{s.t. } y_1 = y, \quad y_m = z, \quad \forall 1 \leq k \leq m-1 \\ & \quad d_X(y_k, y_{k+1}) \leq \epsilon. \end{aligned} \quad (21)$$

Once possible sets are constructed, we search for a global correspondence between candidates of each set. Since the number of sets is small, the search becomes feasible. In many practical problems, exhaustive search is possible. In cases where search complexity is still prohibitive we use a branch and bound algorithm similar to [14]. While complexity remains the same, the search space becomes extremely small in practice.

5.3. Generalized MDS

Once a coarse match is found, it is used as an initialization of the second refinement stage. Solving (15) requires to find a correspondence which distorts the metric the least. Following the discretization in [5], for N mesh points x_i on \hat{X} we search for x'_i locations, (not necessarily coincide with the mesh vertices), with similar diffusion distances between them, minimizing

$$\min_{x'_1, \dots, x'_N \in \hat{X}} \max_{i, j=1, \dots, N} \left| \hat{d}_{ij} - \hat{d}_X(x'_i, x'_j) \right|^2. \quad (22)$$

We use the convex optimization scheme presented in [5], referred to as generalized multidimensional scaling (GMDS), to solve (22).

6. Experimental results

In order to show the advantages using diffusion distances, we performed several experiments on meshes taken from the TOSCA dataset [7]. The first coarse matching exploration stage took a couple of seconds per surface, and the second stage using GMDS refinement procedure took less than a minute for approximately 2000 points on a Pentium Core 2 Duo 3.0 GHz CPU. We used several time steps to calculate the diffusion distances. Best results were received for $t = 100$.

Figure 1 shows the best five coarse symmetries of a human body undergoing several topology changes. The reflective symmetry (E) is found as well as additional twists (B,C,D). In a small number of points false negatives appear, and these can be rejected using either the GMDS procedure, adding descriptors, or increasing the sample size.

Figure 2 depicts symmetries constructed by using GMDS. We used L_2 instead of L_∞ in the process, which provided better numerical results. Each blue line represents a possible match from a set of 128 matches. We show several matches on semi-transparent human bodies. We calculated self-matching on three different meshes with and without topology changes, of different strengths (A-C), using geodesic and diffusion distances. Four experiments were performed for each mesh, and the quality of the correspondence with and without a topology change, for geodesic and diffusion distances, was measured in terms of the geodesic distances from the ground truth. For ground truth x_i points and \hat{x}_i calculated positions we quantified the correspondence quality by

$$d_C(x, \hat{x}) = \frac{\sum_i d_X(x_i, \hat{x}_i)}{n \cdot \text{Diam}(X)}, \quad (23)$$

where $\text{Diam}(X)$ is the diameter of X and n is the number of points used in the optimization stage, which produces a scaling and sampling invariant measure.

Correspondence quality is summarized in Table 1. Without topology changes both diffusion distances and geodesic distances produce good results, but with the presence of topology changes the performance of geodesic distances is highly degraded while diffusion distances keep their accuracy. For example, in mesh (C) the topology change caused a decrease in correspondence accuracy by 33% using diffusion distances, and by more than 4 times when using geodesic distances.

Figure 3 depicts the *local shape asymmetry* of a human body with local asymmetry introduced by deforming one of the palms followed by adding a topology change, marked

	w/o topology		w/ topology	
	Geo	Diff	Geo	Diff
A	0.0091	0.0094	0.0156 (71%)	0.0126 (34%)
B	0.0187	0.0125	0.0243 (30%)	0.0125 (11%)
C	0.0160	0.0222	0.0901 (463%)	0.0222 (33%)

Table 1. Correspondence quality measured by $d_C(x, \hat{x})$ (23) on three different meshes with and without a topology change, using geodesic and diffusion distances. We added the percentage decrease in accuracy, due to topology changes, in parentheses. The meshes can be seen in Figure 2.

with a black circle. Even though the body does not exhibit non-trivial extrinsic symmetries, we were still able to find its local intrinsic asymmetry, marked with an arrow. High asymmetry values are shaded in blue. We extracted a non-trivial intrinsic symmetry that appeared as an intrinsic reflection, and then used that mapping to detect the abnormality at the palm. The method had difficulties locating asymmetric parts using geodesic distances, yet succeeded using diffusion distances.

Figure 4 presents an extrinsic reflective symmetry calculated from pairs of matching points. We assumed the shape was extrinsically symmetric, and calculated the reflective plane using Principle Component Analysis (PCA) on the centers of the connecting lines between matched points. Adding a topology change rotated the reflective plane by almost 10 degrees when geodesic distances were in use, but only by one degree while using diffusion distances.

For a given metric d , which is t time depended, and a given ϵ , we can sample the space of all possible symmetries $\text{Sym}_\epsilon(X, d)$. We measure the distance between mappings according to (9), and embed this abstract space into \mathbb{R}^2 using multidimensional scaling (MDS) method.

Since the space is obviously non-Euclidean, there are distortions in the process, yet, the visual results are informative. In Figure 5 we continued sampling the symmetries of a human body from Figure 1. We computed 155 potential candidates, calculated their distortion, embedded them in \mathbb{R}^2 using classical MDS, and interpolated their distortion on a plane. We see that the symmetry space itself has one approximate reflective symmetry, indicating that a reflective symmetry is the only true symmetry of the shape. In addition, in Figure 6 we present the influence of ϵ on the symmetry space.

7. Conclusions

We presented a method to extract approximate intrinsic symmetries of bendable surfaces which are topology aware, using diffusion distances. We showed how local asymmetry values can be used for detecting shape abnormalities, and presented a visualization of the entire symmetry space.



Figure 1. Coarse symmetries of a human body. Similar parts appear in similar colors, and the total distortion is indicated as a numerical value. The distortion less identity symmetry is (A). The full reflective symmetry is (E) while (B), (C), and (D) represent possible symmetries with partial reflection. Black circles on the left picture mark points where topology changes were introduced.

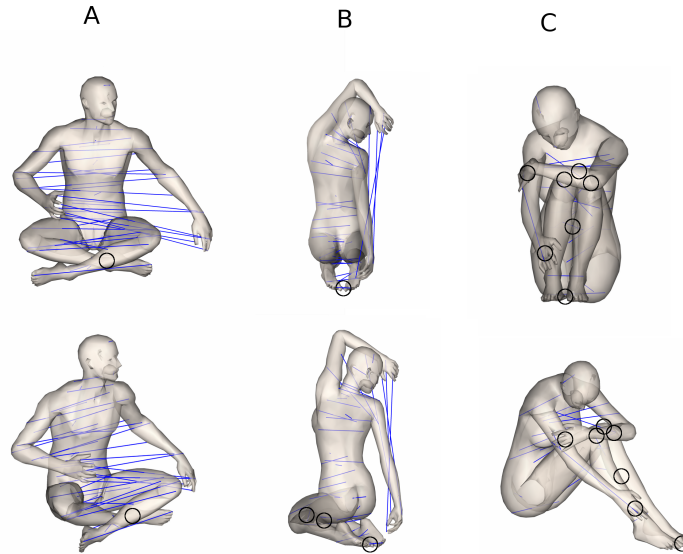


Figure 2. GMDS self-embeddings. Matching points are connected with a blue line on partial transparent human bodies. (A) poses small topology changes, (B) mediocre, and (C) extreme ones. Black circles are drawn over connectors which caused topology changes.

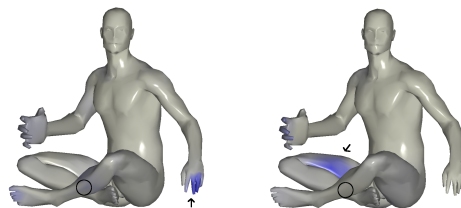


Figure 3. Calculating local asymmetry values for a possible reflective symmetry, using geodesic distances (right) and diffusion distances (left). The right palm was stretched and a topology change was inflicted on the legs. A black circle represents the inflicted topology change, and an arrow represents the high asymmetry area of the object. Blue color represents local asymmetry. The asymmetry in the palm was detected using diffusion distances (left) but could not be isolated using geodesic distances (right).

8. Acknowledgements

This research was supported in part by The Israel Science Foundation (ISF) grant number 623/08, and by The USA Office of Naval Research (ONR) grant. Sapiro is partially supported by ARO, NGA, ONR and NSF.

References

- [1] H. Alt, K. Mehlhorn, H. Wagener, and E. Welzl. Congruence, similarity, and symmetries of geometric objects. *Discrete and Computational Geometry*, 3:237–256, 1988. 1
- [2] M. J. Atallah. On symmetry detection. *IEEE Trans. Computers*, c-34(7), July 1985. 1
- [3] M. Belkin and P. Niyogi. Laplacian eigenmaps for dimensionality reduction and data representation. *Neural Comput.*,

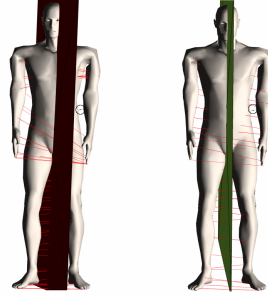


Figure 4. Extrinsic reflective symmetry calculated from matching pairs of points using geodesic (left) and diffusion (right) distances. A topology noise is marked in a black circle, and matching points by a red line. Compared to an accurate reflective plane, the topological noise rotated the plane by 9.8 degrees while using geodesic distances, and by 1.2 degrees for diffusion distances.

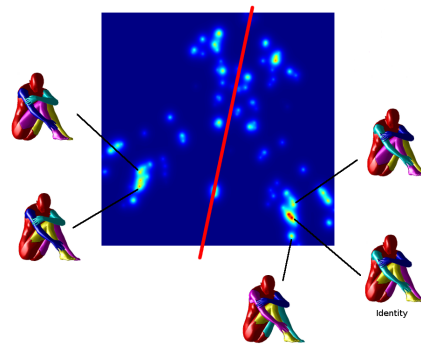


Figure 5. The symmetry space of a the human body from Figure 1 embedded in \mathbb{R}^2 . Red represent low distortion embeddings (symmetries). The red line shows the reflective symmetry of the space itself. We measured the distance between functions according to (9).

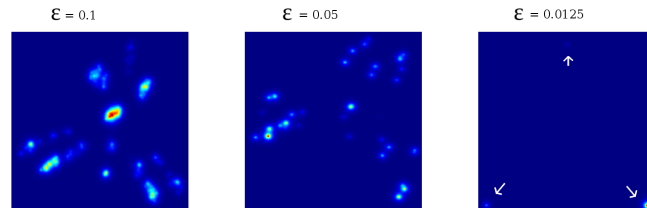


Figure 6. ϵ influence on the symmetry space of the human body from Figure 2 embedded in \mathbb{R}^2 . As ϵ grows, more symmetries appear, but the symmetry space remains symmetric.

- 15(6):1373–1396, 2003. 1
- [4] A. Bobenko and B. Springborn. A discrete laplace–beltrami operator for simplicial surfaces. *Discrete and Computational Geometry*, 38(4):740–756, 2007. 4
- [5] A. M. Bronstein, M. M. Bronstein, and R. Kimmel. Efficient computation of isometry-invariant distances between surfaces. *SIAM Journal on Scientific Computing*, 28/5:1812–1836, 2006. 1, 3, 4, 5
- [6] A. M. Bronstein, M. M. Bronstein, and R. Kimmel. Generalized multidimensional scaling: a framework for isometry-invariant partial surface matching. *Proceedings of the National Academy of Sciences (PNAS)*, 103(5):1168–1172, January 2006. 1
- [7] A. M. Bronstein, M. M. Bronstein, and R. Kimmel. *Numerical Geometry of non-rigid shapes*. Springer-Verlag, 2008. 5
- [8] A. M. Bronstein, M. M. Bronstein, R. Kimmel, M. Mahmoudi, and G. Sapiro. A Gromov-Hausdorff framework with diffusion geometry for topologically-robust non-rigid shape matching. *International Journal of Computer Vision (IJCV)*, 2009. 2
- [9] D. Burago, Y. Burago, and S. Ivanov. *A course in metric*

- geometry, volume 33 of *Graduate studies in mathematics*. American Mathematical Society, 2001. 3
- [10] R. R. Coifman, S. Lafon, A. B. Lee, M. Maggioni, B. Nadler, F. Warner, and S. W. Zucker. Geometric diffusions as a tool for harmonic analysis and structure definition of data: Diffusion maps. *Proc. National Academy of Sciences*, 102(21):7426–7431, 2005. 2
- [11] A. Elad and R. Kimmel. On bending invariant signatures for surfaces. *IEEE Trans. on Pattern Analysis and Machine Intelligence (PAMI)*, 25(10):1285–1295, 2003. 1, 3
- [12] M. Floater and K. Hormann. Surface parameterization: a tutorial and survey. *Advances in multiresolution for geometric modelling*, 1, 2005. 4
- [13] R. Gal, A. Shamir, and D. Cohen-Or. Pose-oblivious shape signature. *IEEE Transactions on Visualization and Computer Graphics*, 13(2):261–271, 2007. 1
- [14] N. Gelfand, N. J. Mitra, L. J. Guibas, and H. Pottmann. Robust global registration. In *Proc. Eurographics Symposium on Geometry Processing (SGP)*, pages 197–206, 2005. 4
- [15] M. Gromov. *Structures métriques pour les variétés riemanniennes*. Number 1 in Textes Mathématiques. 1981. 1, 3
- [16] A. Hamza and H. Krim. Probabilistic shape descriptor for triangulated surfaces. In *Proc. IEEE International Conference on Image Processing (ICIP)*, volume 1, pages 1041–1044, Sept. 2005. 1
- [17] D. Hochbaum and D. Shmoys. A best possible heuristic for the k-center problem. *Mathematics of Operations Research*, 10(2):180–184, May 1985. 4
- [18] P. Jones, M. Maggioni, and R. Schul. Manifold parametrizations by eigenfunctions of the laplacian and heat kernels. *Proceedings of the National Academy of Sciences (PNAS)*, 105(6):1803, 2008. 2
- [19] M. Kazhdan, B. Chazelle, D. Dobkin, T. Funkhouser, and S. Rusinkiewicz. A reflective symmetry descriptor for 3D models. *Algorithmica*, 38(1):201–225, 2003. 1
- [20] D. Knossow, A. Sharma, D. Mateus, and R. P. Horaud. Inexact matching of large and sparse graphs using laplacian eigenvectors. In *Proceedings 7th Workshop on Graph-based Representations in Pattern Recognition*, LNCS 5534, May 2009. 1
- [21] S. Lafon. Diffusion Maps and Geometric Harmonics. *Ph.D. dissertation, Yale University*, 2004. 2
- [22] B. Lévy. Laplace-Beltrami eigenfunctions towards an algorithm that “understands” geometry. In *Int’l Conf. Shape Modeling and Applications*, 2006. 4
- [23] M. Mahmoudi and G. Sapiro. Three-dimensional point cloud recognition via distributions of geometric distances. *Graphical Models*, 71(1):22–31, 2009. 1, 4
- [24] G. Marola. On the detection of axes of symmetry of symmetric and almost symmetric planner images. *IEEE Trans. on Pattern Analysis and Machine Intelligence (PAMI)*, 11(1), Jan. 1989. 1
- [25] F. Mémoi. Spectral Gromov-Wasserstein distances for shape matching. In *Workshop on Non-Rigid Shape Analysis and Deformable Image Alignment (NORDIA)*, october 2009. 1
- [26] F. Mémoi and G. Sapiro. A theoretical and computational framework for isometry invariant recognition of point cloud data. *Foundations of Computational Mathematics*, 5:313–346, 2005. 1, 3
- [27] N. J. Mitra, L. J. Guibas, and M. Pauly. Partial and approximate symmetry detection for 3D geometry. In *Proc. International Conference and Exhibition on Computer Graphics and Interactive Techniques (SIGGRAPH)*, pages 560–568, 2006. 1
- [28] M. Ovsjanikov, A. M. Bronstein, M. M. Bronstein, and L. Guibas. Shape google: a computer vision approach for invariant retrieval of non-rigid shapes. In *Workshop on Non-rigid Shapes and Deformable Image Alignment (NORDIA)*, 2009. 2
- [29] M. Ovsjanikov, J. Sun, and L. Guibas. Global intrinsic symmetries of shapes. In *Proc. Eurographics Symposium on Geometry Processing (SGP)*, volume 27, 2008. 1
- [30] M. Pauly, N. Mitra, J. Wallner, and H. P. L. Guibas. Discovering structural regularity in 3d geometry. In *Proc. International Conference and Exhibition on Computer Graphics and Interactive Techniques (SIGGRAPH)*, pages 1–11, 2008. 1
- [31] U. Pinkall and K. Polthier. Computing discrete minimal surfaces and their conjugates. *Experimental mathematics*, 2(1):15–36, 1993. 4
- [32] D. Raviv, A. M. Bronstein, M. M. Bronstein, and R. Kimmel. Symmetries of non-rigid shapes. In *Proc. Workshop on Non-rigid Registration and Tracking (NRTL)*, Oct. 2007. 1, 4
- [33] D. Raviv, A. M. Bronstein, M. M. Bronstein, and R. Kimmel. Full and partial symmetries of non-rigid shapes. *International Journal of Computer Vision (IJCV)*, 2009. 1
- [34] M. Reuter, S. Biasotti, D. Giorgi, G. Patanè, and M. Spagnuolo. Discrete laplace-beltrami operators for shape analysis and segmentation. *Computers & Graphics*, 33:381–390, 2009. 1, 4
- [35] M. Reuter, F.-E. Wolter, and N. Peinecke. Laplace beltrami spectra as shape-dna of surfaces and solids. *Computer-Aided Design*, 38:342–366, 2006. 1
- [36] Y. Rubner, C. Tomasi, and L. J. Guibas. The earth mover’s distance as a metric for image retrieval. *International Journal of Computer Vision*, 40(2):99–121, 2000. 4
- [37] R. M. Rustamov. Laplace-beltrami eigenfunctions for deformation invariant shape representation. In *Proc. Eurographics Symposium on Geometry Processing (SGP)*, pages 225–233, 2007. 1
- [38] J. Sun, M. Ovsjanikov, and L. Guibas. A Concise and Provably Informative Multi-Scale Signature Based on Heat Diffusion. In *Proc. Eurographics Symposium on Geometry Processing (SGP)*, 2009. 2
- [39] K. Xu, H. Zhang, A. Tagliasacchi, L. Liu, G. Li, M. Meng, and Y. Xiong. Partial intrinsic reflectional symmetry of 3D shapes. In *Proc. International Conference and Exhibition on Computer Graphics and Interactive Techniques (SIGGRAPH)*, 2009. 1
- [40] H. Zabrodsky, S. Peleg, and D. Avnir. Symmetry as a continuous feature. *IEEE Trans. on Pattern Analysis and Machine Intelligence (PAMI)*, 17(12):1154–1166, 1995. 2
- [41] H. Zhang. Discrete combinatorial Laplacian operators for digital geometry processing. In *SIAM Conference on Geometric Design*, pages 575–592, 2004. 4